Band-pass processing in a GPCR signalling pathway selects for NFAT transcription factor activation†

M. Sumit,[ab] R. R. Neubig,[c] S. Takayama[*adef] and J. J. Linderman[*eg]

†Electronic Supporting Information (ESI)

a Biointerface Institute, North Campus Research Complex, University of Michigan, 2800 Plymouth Road, Ann Arbor, MI 48109, USA
b Biophysics Graduate Program, University of Michigan, Ann Arbor, MI 48109, USA
c Department of Pharmacology and Toxicology, Michigan State University, 1355 Bogue Street, East Lansing, MI 48824, USA
d Michigan Centre for Integrative Research in Critical Care, North Campus Research Complex, University of Michigan, 2800 Plymouth Road, Ann Arbor, MI 48109, USA
e Department of Biomedical Engineering, University of Michigan, 1107 Carl A. Gerstacker Building, 2200, Bonisteel Blvd, Ann Arbor, MI 48109, USA. E-mail: takayama@umich.edu
f Macromolecular Science and Engineering Program, University of Michigan, 2300, Hayward Street, Ann Arbor, MI 48109, USA
g Department of Chemical Engineering, University of Michigan, Building 26, 2800 Plymouth Road, Ann Arbor, MI 48109, USA. E-mail: linderma@umich.edu

Text S1. *Brief description of the model*

The mathematical model for GPCR-calcium-NFAT signaling can be described in two modules as follows:

a. GPCR-calcium signaling: Our GPCR-calcium model incorporates ligand (CCh), GPCR (M_3), G-protein, phospholipase C (PLC), inositol triphosphate (IP_3) and calcium dynamics and is based on previous work [1,2]. Briefly, CCh binds to M3 muscarinic receptors, promoting G-protein coupling. Following the exchange of GDP for GTP on the alpha-subunit (Gα), Gα dissociates from the receptor and binds to PLC, initiating downstream signaling. GTP on activated Gα is rapidly hydrolyzed to GDP, forming inactive Gα-GDP. If Gα is bound to PLC, then this hydrolysis reforms inactive PLC as well as inactive Gα. The ligand-receptor complex (L-R) is reversibly phosphorylated to form inactive L-R-P state. The inactive complex can be dephosphorylated to reform the free receptor or can be internalized and either degraded or recycled back to the surface via endosomal sorting [3]. Gα binding to PLC increases IP3 production; IP3 binds to the inositol triphosphate receptor (IP3R) on the endoplasmic reticulum (ER), triggering the release of Ca^{2+} from ER into the cytosol. Cytosolic Ca^{2+} acts both to stimulate and to inhibit its release from the ER through multiple pathways. The oscillatory release of Ca^{2+} from the ER is achieved by the SERCA pump, which pumps cytosolic Ca^{2+} back into the ER. Ca^{2+} can also enter or leave the cell through the plasma membrane.

b. Calcium-NFAT signaling: Our GPCR-calcium model was modularly combined with a calcium-NFAT4 model based on Tomida et al [4] and Cooling et al [5]. Briefly, the rise in cytoplasmic Ca^{2+} activates calcineurin, which binds to cytoplasmic phosphorylated NFAT ($NFATpi_{cyto}$) and leads to dephosphorylation ($NFAT_{cyto}$). The complex can either form inactive calcineurin and cytoplasmic $NFATpi_{cyto}$ upon rephosphorylation, or the calcineurin-dephosphorylated NFAT complex may translocate to the nucleus because of the exposure of the nuclear localization signal domain upon dephosphorylation. Nuclear dephosphorylated NFAT ($NFAT_{nuc}$) is the active form for NFAT that binds with DNA at specific sites and, along with other transcription factors, brings about a variety of physiological responses. $NFAT_{nuc}$ may then undergo phosphorylation to form inactive nuclear phosphorylated NFAT ($NFATpi_{nuc}$) which then translocates back to the cytoplasm.

Text S2. *Variables, Parameters and Equations for GPCR-Calcium-NFAT4 model*

Variable	Initial Value	Units^	Description
R	0.07	μM	Free M3 receptors
L	Input	μM	Extracellular carbachol (ligand)
C	0	μM	Ligand/receptor complex
C_p	0	μM	Phosphorylated C
R_{int}	0	μM	Internalized Receptor
G_T	0.2	μM	Inactive G-protein
G_{GTP}	0	μM	GTP-bound alpha-subunit
G_{GDP}	0	μM	GDP-bound alpha-subunit
$\beta\gamma$	0	μM	Beta-gamma dimer subunit
$\beta\gamma_{int}$	0	μM	Beta-gamma subunit internalized
PLC_T	0.1	μM	Inactive PLC
$PLC*$	0	μM	Activated PLC (bound to G_{GTP})
IP_3	0.03	μM	Inositol trisphosphate
$f_{IP_3R_a}$	0.9	-	Fraction of active IP_3R vs total
Ca_{ER}	2.9	μM	Calcium in endoplasmic reticulum
$Ca_{cytosol}$	0.03	μM	Calcium in cytosol
$NFATpi_{cyto}$	1.22	nM	Cytoplasmic phosphorylated NFAT
$NFAT_{cyto}$	0.01	nM	Cytoplasmic dephosphorylated NFAT
$NFAT_{nuc}$	0.25	nM	Nuclear dephosphorylated NFAT
$NFATpi_{nuc}$	0.0035	nM	Nuclear phosphorylated NFAT

Ligand-binding and G-protein kinetics

Parameter	Model Value	Units	Description	Literature Value	Ref.
$k_{f,L}$	2.27	$\mu M^{-1}s^{-1}$	Rate constant for binding of L to R	0.8 – 5.1	[6–9]
$k_{r,L}$	0.07	s^{-1}	Rate constant for dissociation of L from C	0.01 – 0.11	[6–9]
k_3	0.0077	s^{-1}	Exchange rate constant of GDP for GTP	0.005 – 0.05	[7,10]
k_4	1.9	s^{-1}	Hydrolysis rate constant of GTP to GDP	0.100 – 2.00	[7,11]
k_5	2.0*10^{-5}	$(\#/cell)^{-1}s^{-1}$	Encounter rate of C and G	2*10^{-5}	[7,11]

k_6	2.0*10^{-5}	$(\#/cell)^{-1}s^{-1}$	Encounter rate of PLC and G_{GTP}	2.0*10^{-5}	[7]
k_7	1.0*10^{-5}	$(\#/cell)^{-1}s^{-1}$	Encounter rate of G_{GDP} and $\beta\gamma$	10^{-5} – 10^{-4}	[7,12]

Receptor desensitization kinetics (adapted from Vayttaden *et al*, 2010 [13] modeled for a different GPCR (Beta Adrenergic Receptor) [#]

Parameter	**Model Value**	**Units**	**Description**
$k_{grk1,f}$	0.029	s^{-1}	Phosphorylation rate constant for C
$k_{grk1,r}$	3.6*10^{-3}	s^{-1}	Dephosphorylation rate constant for C_p
k_{int}	0.0037	s^{-1}	Rate constant for internalization of C_p
k_{deg}	0.0004	s^{-1}	Rate constant for degradation of internalized receptors
k_{rec}	0.001	s^{-1}	Receptor recycle rate constant

Calcium and IP$_3$ kinetics (adapted from Politi *et al*, 2006 [2]) [#]

Parameter	**Model Value**	**Units**	**Description**
V_{serca}	0.267	$\mu M^{-1}s^{-1}$	Maximal SERCA pump rate
K_{serca}	0.076	μM	Half-activation constant of SERCA pump
V_{pm}	0.0138	$\mu M^{-1}s^{-1}$	Maximal PMCA pump rate
K_{pm}	0.0756	μM	Half-activation constant of PMCA pump
v_0	10^{-4}	$\mu M^{-1}s^{-1}$	Basal calcium flux into cell
ϕ	0.0024	s^{-1}	Stimulant-dependent calcium flux into cell
ε	3	a.u.	Calcium flux strength
$beta$	0.185	a.u.	Ratio of effective volume of endoplasmic reticulum to cytosol
P	1.7	a.u.	Hill coefficient for PLC-Calcium binding
k_{ca}	950	s^{-1}	Activated rate constant of IP_3 synthesis per molecule of PLC
k_{basal}	0.3	$\mu M^{-1}s^{-1}$	Rate constant for basal IP_3 synthesis
k_{3k}	0	s^{-1}	Phosphorylation rate of IP_3
K_{3k}	0.465	μM	Half activation constant of IP_3-kinase
k_{5p}	0.56	s^{-1}	Dephosphorylation rate of IP_3
K_{plc}	0.213	μM	Half-activation constant of PLC

k_1	0.85	s^{-1}	Maximal rate constant of calcium release through IP_3R
k_2	0.014	s^{-1}	Rate constant for calcium leak through IP_3R
K_a	0.059	μM	Equilibrium constant of calcium binding to activating site on IP_3R
K_i	0.47	μM	Equilibrium constant of calcium binding to inhibiting site on IP_3R
K_p	0.13	μM	Equilibrium constant of IP_3 binding to IP_3R
τ_r	7	s	Characteristic time of IP_3R inactivation

Calcium-NFAT dynamics (adapted from Cooling *et al*, 2009 [5]) [#]

kd1	1760	*nM*	Calcineurin-Calmodulin dissociation constant
kn1	$7.7*10^{-6}$	$(nM\text{-}s)^{-1}$	Rate constant for association of activated calcineurin and $NFATpi_{cyto}$
kn2	0.002	s^{-1}	Rate constant for dissociation of $NFATpi_{cyto}$ from Calcineurin-$NFAT_{cyto}$ complex
kn3	$1.0*10^{-3}$	s^{-1}	Rate constant for nuclear translocation of activated NFAT [&]
kn4	$4.45*10^{-4}$	s^{-1}	Dissociation rate of activated nuclear NFAT
kn5	$4.71*10^{-5}$	$(nM\text{-}s)^{-1}$	Rate constant for association of nuclear NFAT and Calcineurin
kn6	0.003 - 0.0003	s^{-1}	Rate constant for back-translocation of nuclear NFAT to the cytoplasm [&]
KmN	535	*nM*	Half-maximal activation coefficient of calcium
M	6000	*nM*	Calmodulin concentration
N_{tot}	2000	*nM*	Total Calcineurin concentration
n	2.92	*a.u.*	Calcineurin hill coefficient
C_cn	8	*a.u.*	Scaling to adjust cytoplasmic versus nuclear volume
Ca_basal	70	*nM*	Basal bound cytoplasmic calcium

[&] parameter values vary for different NFAT isoforms; adjusted and optimized based on determined experimental values in [4,14].

[#] Parameter values were determined by searching the parameter space using Latin Hypercube Sampling and choosing the values that best fit the experimental data. The values are either same or are of the same order of magnitude as the reference.

$^{\wedge} conv = 3.1725 \times 10^{-6} \frac{\mu M}{\#/cell}$, used to convert units

Model Reactions	Description
Ligand-Receptor kinetics	
$v_1 = k_{f,L}[L][R] - k_{r,L}[C]$	Rate of ligand binding free receptor $(\mu M/s)$
$v_2 = k_{grk1,f}[C] - k_{grk1,r}[C_P] \times conv$	Rate of phosphorylation of C $(\mu M/s)$
$v_{int} = k_{int}[C_p]$	Rate of receptor internalization
$v_{deg} = k_{deg}[R_{int}]$	Rate of degradation of internalized receptors
$v_{rec} = k_{rec}[R_{int}]$	Rate of receptor recycling
G-protein kinetics and PLC activation	
$v_5 = k_3[G]$	Exchange rate of GTP for GDP on alpha subunit of G $(\mu M/s)$
$v_6 = \frac{k_5}{conv}[G][C]$	Encounter rate of G with C to form G_{GTP} $(\mu M/s)$
$v_7 = \frac{k_6}{conv}[G_{GTP}][PLC]$	Encounter rate of G_{GTP} with PLC to form PLC^* $(\mu M/s)$
$v_8 = k_4[G_{GTP}]$	Rate of hydrolysis of G_{GTP} to G_{GDP} $(\mu M/s)$
$v_9 = k_4[PLC^*]$	Rate of inactivation of PLC^* to PLC $(\mu M/s)$
$v_{10} = \frac{k_7}{conv}[G_{GDP}][\beta\gamma]$	Encounter rate of G_{GDP} with $\beta\gamma$ $(\mu M/s)$
IP_3-calcium kinetics	
$v_{11} = (k_{ca}[PLC^*] + k_{basal})\left(\frac{[Ca_{cyt}]^p}{[Ca_{cyt}]^p + K_{plc}{}^p}\right)$	Rate of IP_3 synthesis $(\mu M/s)$
$v_{12} = \left(k_{3k}\left(\frac{[Ca_{cyt}]^2}{[Ca_{cyt}]^2 + K_{3k}{}^2}\right) + k_{5p}\right)[IP_3]$	Rate of IP_3 degradation $(\mu M/s)$
$v_{13} = \left(k_1\left(f_{IP_3R_a}\left(\frac{[Ca_{cyt}]}{[Ca_{cyt}]+K_a}\right)\left(\frac{[IP_3]}{[IP_3]+K_p}\right)\right)^3 + k_2\right)\left([Ca_{ER}] - [Ca_{cyt}]\right)$	Rate of Ca_{ER} release into cytosol $(\mu M/s)$
$v_{14} = V_{serca}\left(\frac{[Ca_{cty}]^2}{[Ca_{cty}]^2 + K_{serca}{}^2}\right)$	Rate of pumping Ca_{cty} back into ER $(\mu M/s)$
$v_{15} = \varepsilon\left(v_0 + \phi^*(k_{ca}[PLC^*] + k_{basal})^* \frac{1}{k_{3k} + k_{5p}} - V_{pm}\left(\frac{[Ca_{cyt}]^2}{[Ca_{cyt}]^2 + K_{pm}{}^2}\right)\right)$	Flux of calcium into and out of cell across plasma membrane $(\mu M/s)$
$v_{16} = \frac{1}{\tau_R}$	Recovery of inactivated IP_3R $(1/s)$

$v_{17} = \frac{f_{IP_3R_a}}{\tau_R}\left(\frac{K_i}{[Ca_{cyt}]+K_i}\right)$	Inactivation of IP_3R $(1/s)$
Calcium-NFAT kinetics	
$Ca = Ca_{basal} + [Ca_{cyt}]$	Total cytoplasmic calcium available for NFAT activation
$actN = \frac{Ca^4}{Ca^4 + KmN^4 * (1 + kd1/M)}$	Fraction of activated calcineurin
$J1 = kn1[NFATpi_{cyto}]N_{tot} * actN - kn2[NFAT_{cyto}](1\text{-}\ actN)$	Flux of Activated NFAT complex formation
$J2 = kn3 * [NFAT_{cyto}]$	Flux of nuclear import of activated NFAT
$J3 = kn4[NFAT_{nuc}](1 - actN) - kn5[NFATpi_{nuc}]N_{tot} * actN)$	Flux of Activated NFAT complex dissociation in the nucleus
$J4 = kn6[NFATpi_{nuc}]$	Flux of nuclear export of phosphorylated NFAT

Model Equations
$[G] = [G_T] - [G_{GTP}] - [PLC^*] - [G_{GDP}]$ - $[\beta\gamma_{int}]$
$[PLC] = [PLC_T] - [PLC^*]$
$[\beta\gamma] = [G_{GTP}] + [PLC^*] + [G_{GDP}]$
$\frac{d[C]}{dt} = v_1 - v_2$
$\frac{d[C_p]}{dt} = \frac{v_2}{conv} - v_{\text{int}}$
$\frac{dR_{int}}{dt} = v_{int} - v_{deg} - v_{rec}$
$\frac{dR}{dt} = -v_1 + conv * v_{rec}$
$\frac{d[G_{GTP}]}{dt} = v_5 + v_6 - v_7 - v_8$
$\frac{d[PLC^*]}{dt} = v_7 - v_9$
$\frac{d[G_{GDP}]}{dt} = v_8 + v_9 - v_{10}$
$\frac{d[IP_3]}{dt} = v_{11} - v_{12}$
$\frac{d[Ca_{cyt}]}{dt} = v_{13} - v_{14} + v_{15}$
$\frac{d[Ca_{ER}]}{dt} = \frac{-v_{13} + v_{14}}{\beta}$

$\frac{d[f_{IP_3R_a}]}{dt} = v_{16} - v_{17}$
$\frac{d[NFATpi_{cyto}]}{dt} = -J1 + J4/C\_cn$
$\frac{d[NFAT_{cyt}]}{dt} = J1 - J2$
$\frac{d[NFAT_{nuc}]}{dt} = J2 * C\_cn - J3$
$\frac{d[NFATpi_{nuc}]}{dt} = J3 - J4$

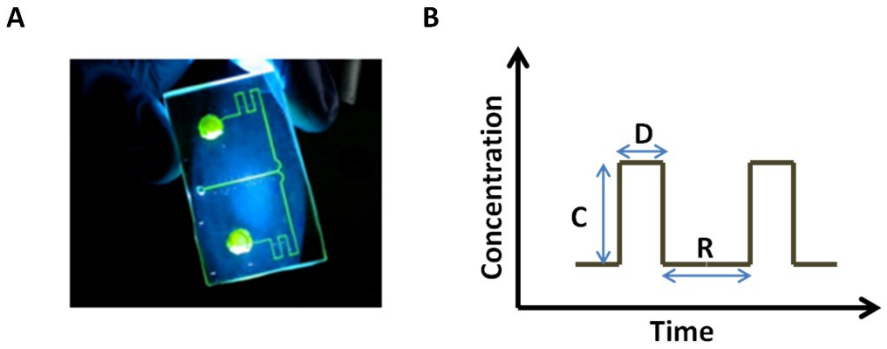

Fig. S1. Braille based pulsatile microfluidics device allows delivery of temporally controlled ligand inputs. A) Braille-pin actuator based PDMS microfluidic device used to deliver time varying pulsatile ligand input to cells seeded in the microfluidic channel; image obtained from Jovic et al [7]. B) The ligand delivery (input) can be controlled in terms of C (concentration), D (duration of stimulation) and R (rest period between two consecutive stimulations).

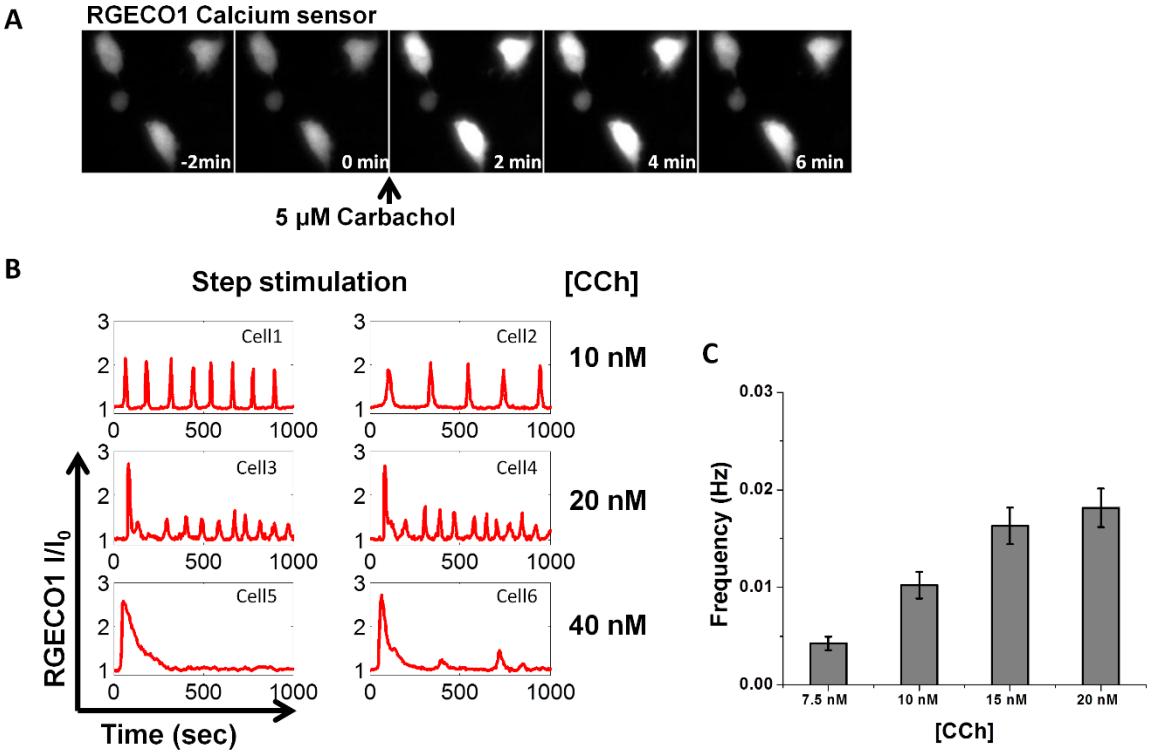

Fig. S2. Oscillatory calcium responses in GPCR-linked calcium signaling can be measured using a calcium sensor RGECO1, transiently transfected into HEK 293 cells. A) Cells stimulated 5 µM with carbachol show increase in RGECO1 intensity. B) Amidst cell-to-cell variability, ligand stimulation leads to calcium response (oscillatory and/or peak and plateau). C. The frequency of calcium oscillation in cells eliciting oscillatory response is dose dependent. Error bars are +/- S.E.M., n > 20 each case.

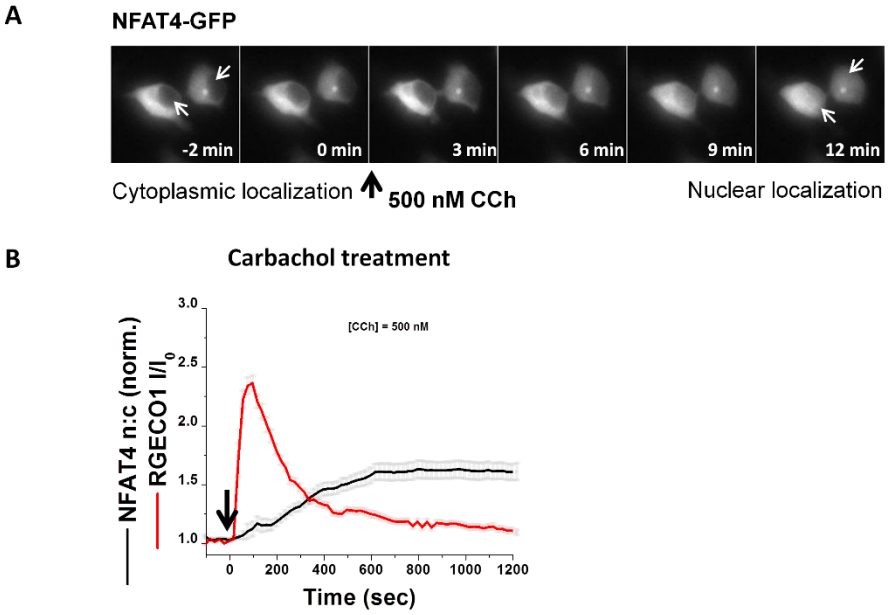

Fig. S3. Carbachol-induced GPCR activation leads to increase in cytoplasmic calcium and subsequently leads to nuclear translocation of NFAT4. A) NFAT4 is primarily localized in the cytoplasm (arrows pointing to the nuclei show relatively much less NFAT4-GFP intensity before carbachol treatment). Upon treatment with 500 nM carbachol, the nuclear intensity gradually increases, indicating nuclear translocation of cytoplasmic NFAT4-GFP. B) Time-resolved dynamics of cytoplasmic calcium and NFAT translocation upon carbachol treatment. Error bars are +/- S.E.M., n>20.

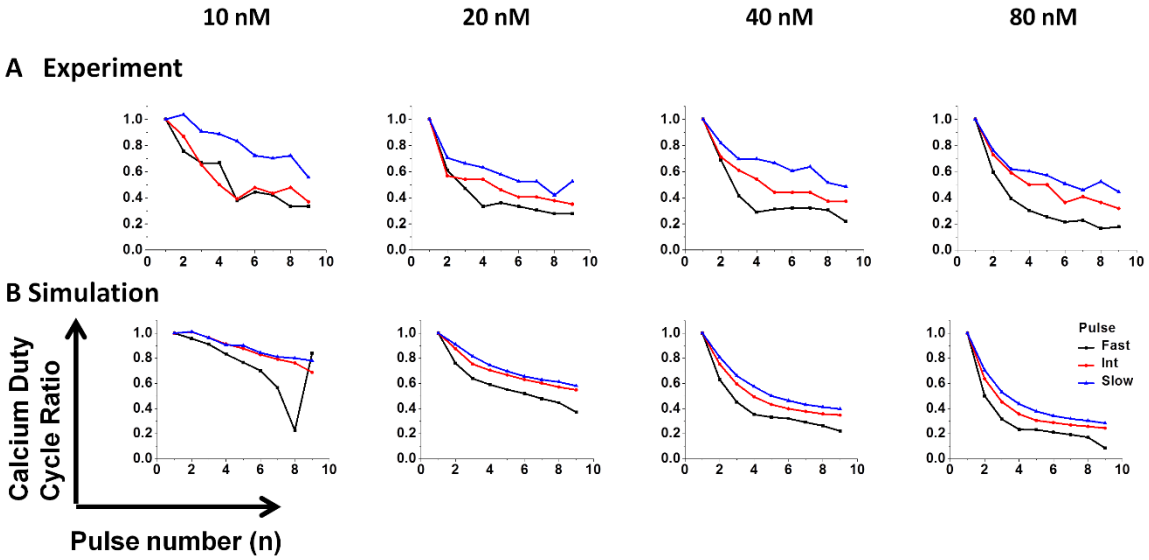

Fig. S4. Calcium Duty Cycle Ratio decays over time upon pulsatile ligand stimulation. A) The calcium duty cycle ratio for the population-averaged calcium response decays faster for fast pulse and vice versa (top panel) indicating frequency modulation. Higher concentrations (left to right: 10 nM, 20 nM, 40 nM and 80 nM respectively) lead to greater extent of decay indicating amplitude modulation. B) Our

mathematical model captures both the frequency and amplitude modulation features as observed experimentally.

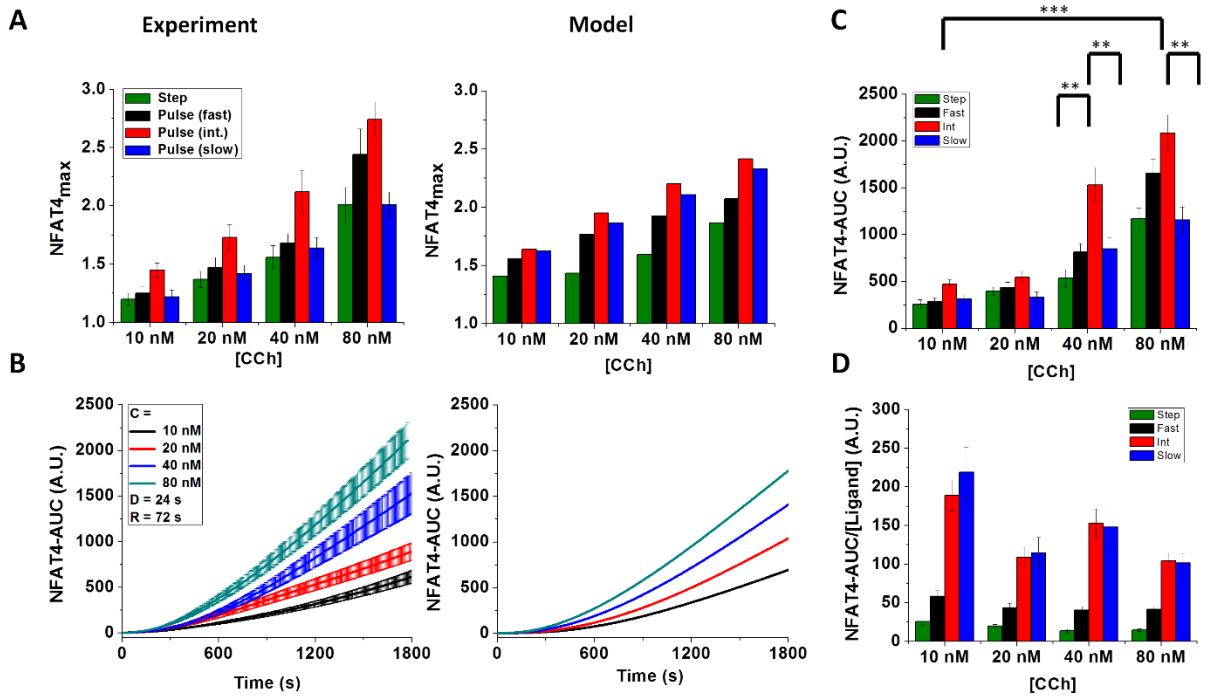

Fig. S5. Nuclear translocation of NFAT4 depends upon pulse frequency as well as amplitude (concentration) of the ligand. A) $NFAT4_{max}$ response is greater for intermediate pulse when compared to slow pulse or fast pulse or step change (left). Our mathematical model captures similar trend as observed experimentally (right). B) Time-dependent NFAT4-AUC response at different concentrations shows amplitude (concentration) dependence of NFAT4 translocation (left). Mathematical model captures similar trend as observed experimentally (right). C) NFAT4-AUC response is greater for intermediate pulse when compared to either slow pulse or fast pulse, similar to $NFAT4_{max}$ response. D) Total NFAT4 response per unit ligand is greater for lower ligand concentrations with slower pulse stimulations. Error bars are +/- S.E.M., n>20.

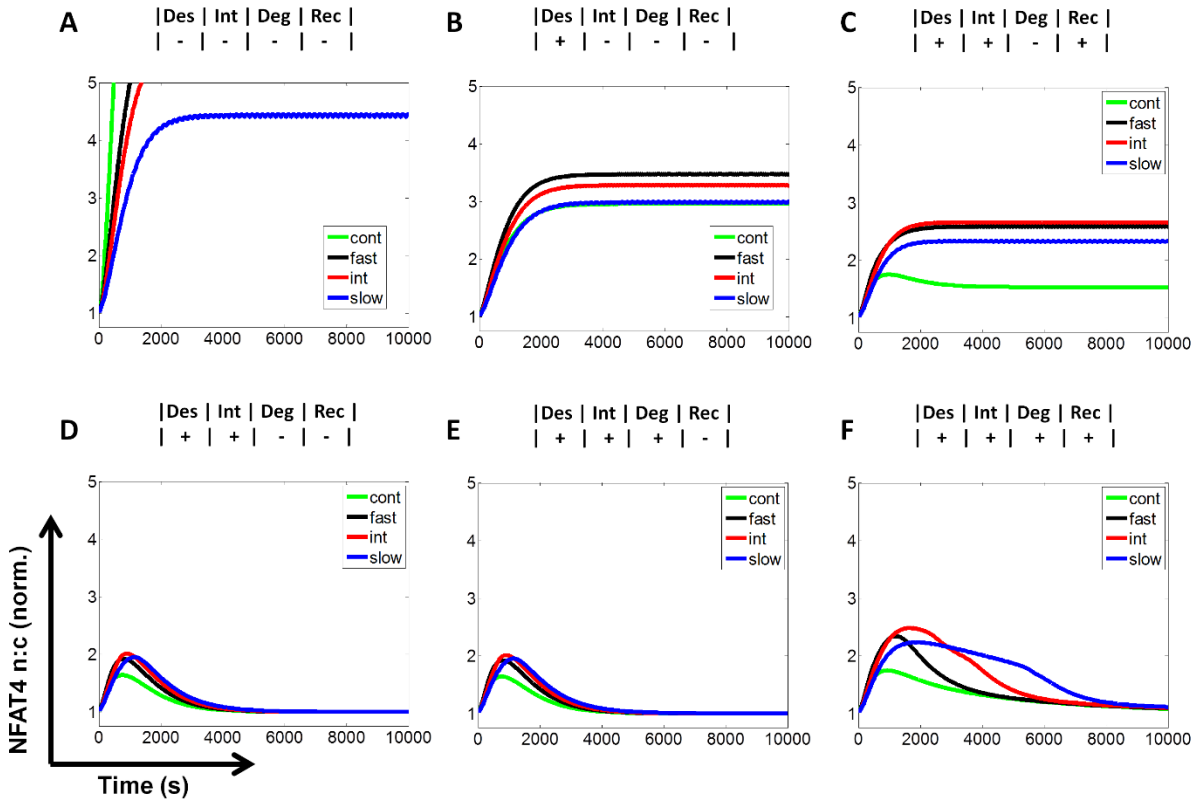

Fig. S6. Analysis of the mathematical model: Turning off receptor regulation modules by setting the corresponding parameter values to zero. (A) Turning off desensitization shoots off the calcium response[1] and also the corresponding NFAT response indicating the receptor desensitization is essential for controlled transcription factor activation (B) Receptor phosphorylation but no receptor internalization leads to calcium oscillations *ad infinitum*, and consequently a high pass bound NFAT4 response. (C) Complete recycling of internalized receptors without ligand mediated receptor degradation shows similar calcium-NFAT response as in (B). (D) & (E) Complete internalization of phosphorylated receptors without any recycling doesn't produce band-pass response for different pulse frequencies. (F) Ligand-mediated endosomal sorting of receptors towards partial degradation and recycling leads to the band-pass response as we observe in the microfluidic experiments. For all cases of simulations, C = 40 nM, and D = 24 s for pulsed stimulations, R = 24 s (fast), 72 s (int.) and 144s (slow).

Table S1. **Sensitivity analysis of the model.** PRCC results (positive and negative correlations) for the receptor parameters[$] (top) and NFAT parameters[$] (bottom) show strong correlations of receptor and NFAT kinetics to the band-pass characteristics (+/-: $p<10^{-3}$, ++/--: $p<10^{-6}$, +++/---: $p<10^{-9}$ with positive or negative correlation).

Band-pass feature	kgrk1f	kgrk1r	kint	kdeg	krec
NFAT_max peak shift	---				++
NFAT_max peak height	---	+++	---	---	+++
Low pass steepness	---	+++	---	---	+++
High pass steepness	---	+++	---	---	+++

Band-pass feature	kn1	kn2	kn3	kn4	kn5	kn6
NFAT_max peak shift	-	--	---	---		--
NFAT_max peak height	---	+++	+++	+++	+++	---
Low pass steepness		+++	+++	+++	+	-
High pass steepness			+++	+++		

[$] ***Abbreviations***: kgrk1f: phosphorylation rate constant of the L-R complex; kgrk1r: dephosphorylation rate constant of phosphorylated L-R complex; kint: rate constant for internalization of the phosphorylated L-R complex; kdeg: rate constant for degradation of internalized L-R-p; krec: rate constant for receptor recycling of internalized L-R-p; kn1: rate constant for association of activated calcineurin and $NFAT4_{cyto}$; kn2: rate constant for dissociation of $NFAT4_{cyto}$ from Calcineurin-$NFAT_{cyto}$ complex; kn3: rate constant for nuclear translocation of activated NFAT; kn4: rate constant for dissociation of activated nuclear NFAT; kn5: rate constant for association of nuclear NFAT and Calcineurin ; kn6: rate constant for back-translocation of nuclear NFAT.

References

1 A. Jovic, S. M. Wade, R. R. Neubig, J. J. Linderman and S. Takayama, *Integr. Biol. (Camb).*, 2013, **5**, 932–9.

2 A. Politi, L. D. Gaspers, A. P. Thomas and T. Höfer, *Biophys. J.*, 2006, **90**, 3120–33.

3 A. R. French and D. A. Lauffenburger, *Biotechnol. Bioeng.*, 1996, **51**, 281–97.

4 T. Tomida, K. Hirose, A. Takizawa, F. Shibasaki and M. Iino, *EMBO J.*, 2003, **22**, 3825–32.

5 M. T. Cooling, P. Hunter and E. J. Crampin, *Biophysj*, 2009, **96**, 2095–2104.

6 G. Schreiber, Y. I. Henis and M. Sokolovsky, *J. Biol. Chem.*, 1985, **260**, 8795–8802.

7 A. Jovic, S. M. Wade, A. Miyawaki, R. R. Neubig, J. J. Linderman and S. Takayama, *Mol. Biosyst.*, 2011, **7**, 2238–2244.

8 M. R. Dowling and S. J. Charlton, *Br. J. Pharmacol.*, 2006, **148**, 927–937.

9 D. A. Sykes, M. R. Dowling and S. J. Charlton, *Mol. Pharmacol.*, 2009, **76**, 543–551.

10 T. Chay and Y. Lee, *J. Theor. Biol.*, 1995, 21–44.

11 W. J. Thomsen and R. R. Neubig, *Biochemistry*, 1989, **28**, 8778–86.

12 P. A. Mahama and J. J. Linderman, *Biophys. J.*, 1994, **67**, 1345–57.

13 S. J. Vayttaden, J. Friedman, T. M. Tran, T. C. Rich, C. W. Dessauer and R. B. Clark, *PLoS Comput. Biol.,* 2010, **6,** e1000647.

14 N. Yissachar, T. S. Fischler, A. A. Cohen, S. Reich-Zeliger, D. Russ, E. Shifrut and Z. Porat, *Mol. Cell*, 2013, **49**, 322–330.